Chem. Res. Chin. Univ. 2013, 29(5), 837—840 doi: 10.1007/s40242-013-3028-4

One-step Synthesis and Gas Sensing Properties of Hierarchical SnO_2 Materials

GUAN Yue[1], WANG Chong[1], WANG Biao[2], MA Jian[1], XU Xiu-mei[1], SUN Yan-feng[1*], LIU Feng-min[1], LIANG Xi-shuang[1], GAO Yuan[1] and LU Ge-yu[1*]

1. State Key Laboratory on Integrated Optoelectronics, College of Electronic Science and Engineering, Jilin University, Changchun 130012, P. R. China;

2. Changchun Institute Optics, Fine Mechanics and Physics, Chinese Academy Sciences, Changchun 130033, P. R. China

Abstract Hierarchical tin oxide(SnO_2) architectures were synthesized with a facile hydrothermal method. In the hydrothermal synthesis, sodium dodecyl benzene sulfonate(SDBS) surfactant plays an important role as structure-directing reagent. The synthesized samples were characterized by powder X-ray diffraction(XRD), field emission scanning electron microscopy(FESEM), transmission electron microscopy(TEM) and high-resolution transmission electron microscopy(HRTEM). The results clearly reveal that the hierarchical architectures of SnO_2 were composed of aggregated nanosheets with a thickness of about 100 nm. A possible mechanism for the formation of the SnO_2 hierarchical architectures was proposed. In addition, the gas sensing properties of the as-prepared products were investigated and it was found that the sensor based on the special SnO_2 hierarchical architectures exhibited a high response and good selectivity to NO_2 at the optimal working temperature of 160 °C.

Keywords Tin oxide; Hydrothermal method; Sodium dodecyl benzene sulfonate(SDBS); NO_2

1 Introduction

Gas sensors based on the semiconductor oxides play an important role in environmental monitoring, chemical process control and personal safety. Semiconductor oxides, such as ZnO, SnO_2, WO_3 and In_2O_3, which were widely chosen as gas sensing materials exhibit excellent sensing properties[1—6]. Among those materials, tin oxide(SnO_2) has been extensively studied due to its high sensitivity and good long-term stability[7]. Besides, it has many applications in other fields such as optoelectronic devices[8,9], transparent conducting electrode[10] and catalyst supports[11]. In particular, two-dimensional SnO_2 nanosheets have attracted much attention due to their remarkable receptivity variation in gaseous environment, excellent lithium storage capacity and cycle performance[12—14].

In this work, novel SnO_2 hierarchical architectures were synthesized with a facile hydrothermal process and the as-prepared products were illustrated in terms of the crystallinity, morphology and structure. Moreover, the dependence of the morphology on reaction time was investigated, and a possible formation mechanism was proposed. Finally, the gas sensing properties of the sensors based on the novel hierarchical SnO_2 to NO_2 were investigated.

2 Experimental

In a typical synthesis process, 0.644 g of $SnSO_4$(3 mmol) was dissolved in 30 mL of deionized water with vigorous stirring for 30 min, then 0.697 g of sodium dodecyl benzene sulfonate(SDBS, 2 mmol) was added in the solution. Having been stirred for 1 h, the mixed solution was transferred into a 50 mL Teflon-lined stainless steel autoclave. The autoclave was maintained at 120 °C for 8 h and then cooled down to room temperature naturally.

The product was collected by centrifugation and washed with distilled water and absolute ethanol, and then dried at 80 °C for 12 h in air. Finally, the product was obtained by calcining at 600 °C for 2 h.

The gas-sensing properties of the samples were determined under laboratory conditions[room humidity: 50%±10%, (23±1) °C]. The measurement was processed by a static process in a test chamber. Environmental air was used as both a reference gas and a diluting gas to obtain desired concentrations of target gases. When the response reached a constant value, the upper cover of the test chamber was removed and the sensor began to recover in air. The response of the sensor was defined as $S=R_g/R_a$ for oxidizing gas or R_a/R_g for reducing gas, where R_a and R_g are the resistances of the sensor in the air and target gas, respectively. The response time and recovery time are defined as the time taken by the sensor to achieve 90% of the total resistance change in the case of adsorption or desorption, respectively.

*Corresponding authors. E-mail: syf@ jlu.edu.cn; lugy@jlu.edu.cn

Received January 14, 2013; accepted March 17, 2013.

Supported by the National Natural Science Foundation of China(Nos.61006055, 61074172, 61134010) and the Program for Changjiang Scholars and Innovative Research Team in University of China(No.IRT1017).

3 Results and Discussion

3.1 Structural and Morphological Characteristics of Prepared SnO_2

The crystal phase of the calcined product was characterized by powder X-ray diffraction(XRD) analysis[Fig.1(A)]. It can be seen from Fig.1(A) that all the peaks of the sample could be well indexed to the tetragonal rutile structure of SnO_2 with lattice parameters of a=0.4738 nm and c=0.3187 nm, which are consistent with the standard data(JCPDS File No. 41-1445). No characteristic peaks from other impurities were detected, indicating the high purity of the product. Furthermore, the strong and sharp diffraction peaks suggest that the products are highly crystalline. Typical scanning electron microscopy (SEM) images of the SnO_2 microspheres are shown in Fig.1(B)—(D) with different magnifications. The low-magnification SEM image of the sample in Fig.2(B) exhibits dispersed microspheres with *ca.* 20 μm in diameter consisted of 3D flower-like nanostructures, while the high magnification SEM image in Fig.1(C) further reveals the flower-like nanostructures constructed from numerous nanosheets. The thickness of each nanosheet is estimated to be about 100 nm a ccording to Fig.1(D).

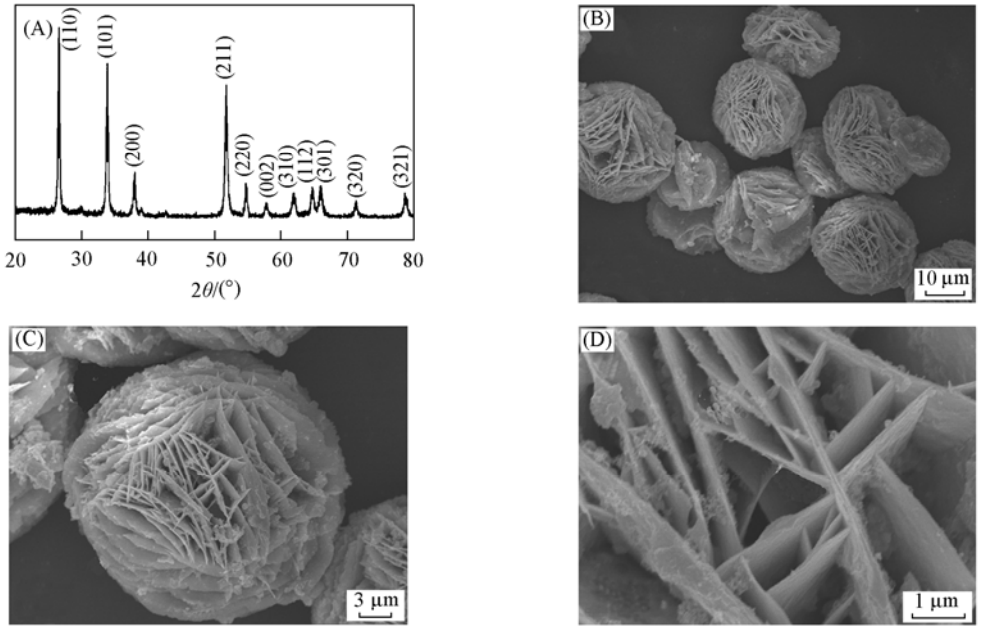

Fig.1 XRD pattern(A), low-magnification(B) and high-magnification(C, D) SEM images of the as-prepared SnO_2 sample

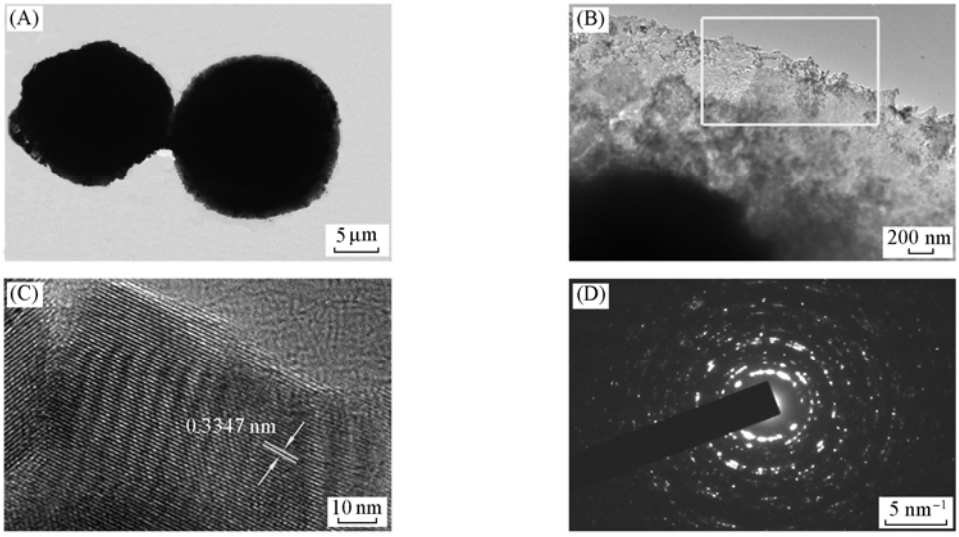

Fig.2 TEM image of the as-prepared SnO_2 sample(A) and typical TEM image(B), HRTEM image(C) and SAED pattern(D) of an individual SnO_2 nanosheet

(C) and (D) are from the fringe marked in image (B).

Further detailed morphology information of the product was obtained with transmission electron microscopy(TEM) and high resolution TEM(HRTEM). The typical TEM images of as-prepared SnO_2 products shown in Fig.2(A) and (B) indicate that the size and shape observed in TEM images are similar to those in the SEM images. The HRTEM image[Fig.2(C)] shows that the spacing between adjacent lattice planes is 0.3347 nm, corresponding to the (110) planes of SnO_2. The selected-area

electron diffraction(SAED) pattern of an individual SnO_2 nanosheet[Fig.2(D)] confirms that the nanosheet is polycrystalline.

3.2 Growth Process and Mechanism of As-prepared SnO_2

To understand the formation process of the SnO_2 hierarchical microstructure and possible growth mechanism, the evolutional morphology of the intermediates obtained at different reaction time was investigated in detail with the results shown in Fig.3. When the hydrothermal time was 2 h, it can be observed that the product was entirely comprised of a relatively uniform nanospheres[Fig.3(A)]. The high-magnification SEM image indicates that the diameters of these nanospheres are about 300 nm[inset in Fig.3(A)]. When the hydrothermal time was prolonged to 6 h, some nanosheet-based hierarchical nanostructures can be clearly observed with *ca.* 10 μm in diameter[Fig.3(B)]. Some of these nanostructures were not fully developed and some separated nanosheets could be detected. When the reaction time was further increased to 8 h, the hierarchical SnO_2 microspheres composed of nanosheets were formed and the diameters were extended to *ca.* 20 μm. The detailed morphology of the product is shown in Fig.1(B)—(D) previously. However, when the reaction time was up to 12 h, the observed sphere was constructed by more nanosheets, which were densely packed, forming a multilayered structure [Fig.3(C)]. The diameter of the sphere was further increased to *ca.* 25 μm.

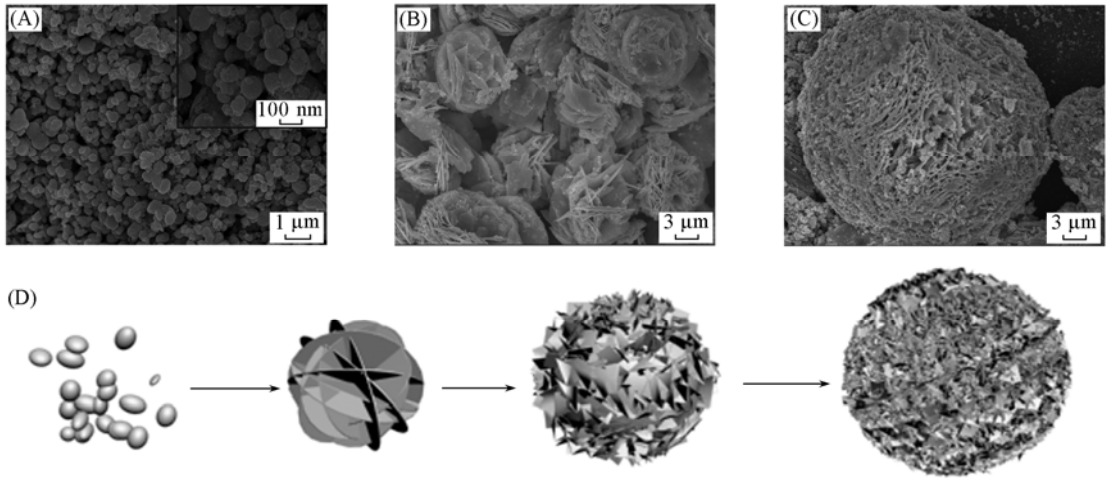

Fig.3 SEM images of morphology evolution of samples prepared at 2(A), 6(B) and 12 h(C) and schematic illustration of the formation process of the prepared hierarchical SnO_2 architectures(D)

The inset of (A) shows the high-magnification SEM image.

According to the above results, it can be concluded that such hierarchical SnO_2 architectures were achieved *via* surfactant-assisted and self-assemble process. SDBS acts as a structure-directing agent for the mineralization of inorganic precursors[15]. The schematic illustration of growth mechanism for the prepared hierarchical SnO_2 architectures under hydrothermal conditions is shown in Fig.3(D). At the initial stage, SnO_2 nuclei formed due to solution supersaturation. The nanoparticles quickly formed and spontaneously aggregated into large spheres for minimizing their surface area. Subsequent crystal growth was initiated preferentially from the active nanoparticles on the surface of the spheres, due to the SDBS surrounding them. In other words, SDBS may act as capping agent to be preferentially absorbed on some certain faces of the nanocrystals, leading to the formation of nanosheets around the spheres. When the reaction time was further progressed, more and more nanosheets assembled to eventually form the as-prepared hierarchical architectures. With increasing the reaction time, the amount of the nanosheets and the diameter of hierarchical architectures increased due to the continual growth of SnO_2 nanocrystal.

3.3 Gas-sensing Properties

For the semiconductor oxide sensors, working temperature is an important factor[16,17]. Fig.4(A) shows the response of sensor to 10 μL/L NO_2 at different working temperatures. The sensor response increases and reaches its maximum at about 160 °C and then decreases rapidly with the increase of the working temperature. The maximum response reaches about 120 at 160 °C, so an optimal operating temperature of 160 °C was chosen to further examine the gas sensing properties. The response and recovery behaviors were investigated by exposing the sensor to NO_2 with different concentrations, as shown in Fig.4(B). The response greatly increased with the increased concentration of NO_2. The responses were about 2, 15, 107, 220, 300 and 385 to 1, 2.5, 5, 20, 50 and 100 μL/L NO_2, respectively. Fig.4(C) shows the dynamic response of the sensor based on the as-prepared SnO_2 architectures to 10 μL/L NO_2. The response time and recovery time to 10 μL/L NO_2 are respectively about 110 and 240 s at 160 °C. The selectivity of the sensor was also invesgated. Fig.4(D) shows the response of the sensor constructed from the as-prepared SnO_2 to various gases, such as H_2S, SO_2, NH_3, H_2, CO, CH_4 and C_2H_5OH. It can be seen clearly that the sensor exhibits the largest response to 10 μL/L NO_2 among the other gases. The sensor exhibited lower responses to H_2S and C_2H_5OH than to NO_2, and was almost insensitive to SO_2, NH_3, H_2, CO and CH_4, indicating that the sensor has a good selectivity for NO_2 within other target gases.

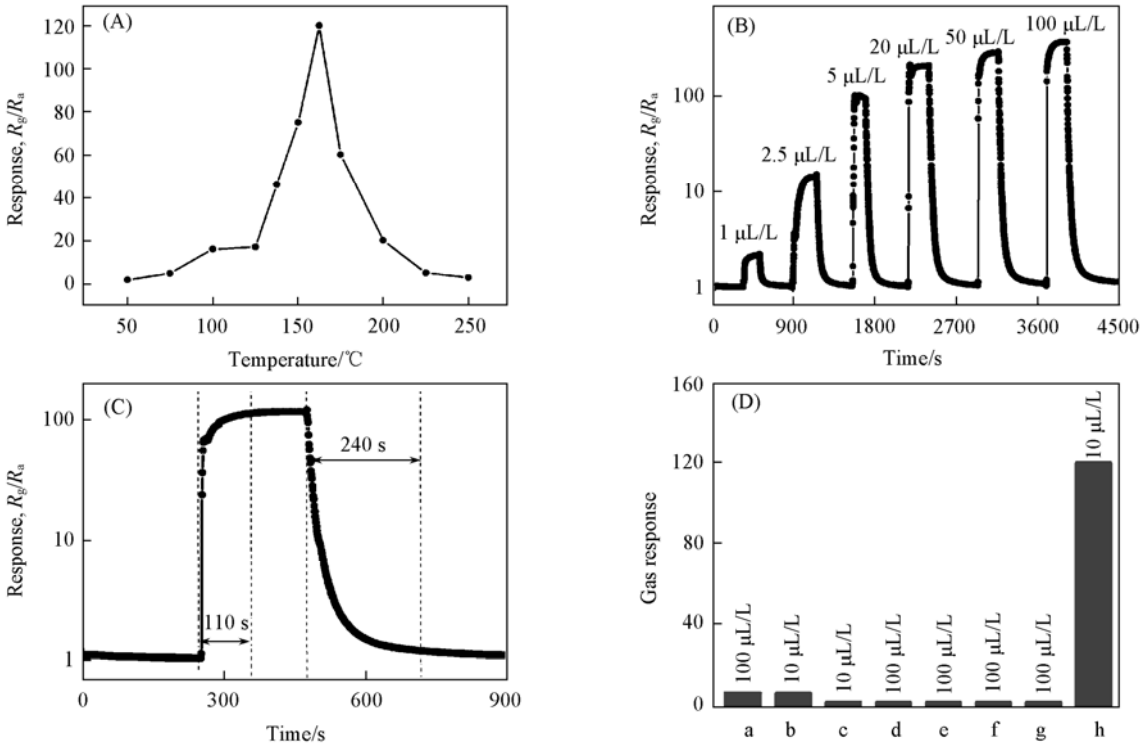

Fig.4 Response of the sensor *vs.* the operating temperature to 10 μL/L NO_2(A), transient response and recovery characteristic of the sensor *vs.* NO_2 concentration at 160 °C(B), dynamic response resistance of the sensor to 10 μL/L NO_2 at 160 °C(C) and response of the sensor to various test gases at 160 °C(D)

(D) a. C_2H_5OH; b. H_2S; c. SO_2, d. NH_3; e. H_2; f. CO; g. CH_4; h. NO_2.

4 Conclusions

The unique hierarchical tin oxide architectures have been synthesized through a facile hydrothermal method. Field emission scanning electron microscopic results indicate that the hierarchical architectures with *ca.* 20 μm in diameter were composed of nanosheets. The characterization and possible formation mechanism of the product were investigated. In addition, the gas sensing properties of as-prepared products were investigated. The sensor based on SnO_2 architectures exhibits a high response and good selectivity to NO_2 gas at 160 °C.

References

[1] Sun P., Yu Y. S., Xu J., *Sens. Actuators B*, **2011**, *160*, 244
[2] Bakrania S. D., Wooldridge M. S., *Sensors*, **2010**, *10*, 7002
[3] Xu X. M., Wang D. W., Wang W. B., *Sens. Actuators B*, **2012**, *171*, 1066
[4] Zhang D. H., Liu Z. Q., Li C., Tang T., Liu X. L., Han S., Lei B., Zhou C. W., *Nano Lett.*, **2004**, *4*, 1919
[5] Xu H. Y., Cui D. L., Cao B. Q., *Chem. Res. Chinese Universities*, **2012**, *28*(6), 1086
[6] Sun P., You L., Sun Y. F., Chen N. K., Li X. B., Sun H. B., Ma J., Lu G. Y., *CrystEngComm*, **2012**, *14*, 1701
[7] Lee J. S., Sim S. K., Min B., Cho K., Kim S. W., Kim S., *J. Cryst. Growth*, **2004**, *267*, 145
[8] Sun J. B., Xu J., Wang B., Sun P., Liu F. M., Lu G. Y., *Chem. Res. Chinese Universities*, **2012**, *28*(3), 483
[9] Korotcenkov G., Cho B. K., Gulina L., Tolstoy V., *Sens. Actuators B*, **2009**, *138*, 512
[10] Wang Y., Lee J. Y., *J. Phys. Chem. B*, **2004**, *108,* 17832
[11] Jia N. Q., Zhou Q., Liu L., Yan M. M., Jiang Z. Y., *J. Electroanal. Chem*., **2005**, *580*, 213
[12] Wu H. B., Chen J. S., Lou X. W., Hng H. H., *J. Phys. Chem. C*, **2011**, *115*, 24605
[13] Masuda Y., Kato K., *J. Cryst. Growth*, **2009**, *311*, 593
[14] Sakaushi K., Oaki Y., Uchiyama H., Hosono E., Zhou H. S., Imai H., *Small*, **2010**, *6*, 776
[15] Zhao Q., Xie Y., Dong T., Zhang Z., *J. Phys. Chem. C*, **2007**, *111*, 11598
[16] Shinde V. R., Gujar T. P., Lokhande C. D., *Sens. Actuators B*, **2007**, *123*, 701
[17] Gong H., Hu J. Q., Wang J. H., Ong C. H., Zhu F. R., *Sens. Actuators B*, **2006**, *115*, 247